

Disturbance observer approach for fuel-efficient heavy-duty vehicle platooning

Gyujin Na, Gyunghoon Park, Valerio Turri, Karl H. Johansson, Hyungbo Shim & Yongsoo Eun

To cite this article: Gyujin Na, Gyunghoon Park, Valerio Turri, Karl H. Johansson, Hyungbo Shim & Yongsoo Eun (2019): Disturbance observer approach for fuel-efficient heavy-duty vehicle platooning, Vehicle System Dynamics, DOI: [10.1080/00423114.2019.1704803](https://doi.org/10.1080/00423114.2019.1704803)

To link to this article: <https://doi.org/10.1080/00423114.2019.1704803>



Published online: 29 Dec 2019.



Submit your article to this journal [↗](#)



Article views: 205




View related articles [↗](#)



View Crossmark data [↗](#)



Disturbance observer approach for fuel-efficient heavy-duty vehicle platooning

Gyujin Na^a, Gyunghoon Park^b, Valerio Turri^c, Karl H. Johansson^c, Hyungbo Shim^d and Yongsoon Eun ^a

^aDepartment of Information and Communication Engineering, DGIST, Daegu, Republic of Korea; ^bCenter for Intelligent and Interactive Robotics, Korea Institute of Science and Technology, Seoul, Republic of Korea; ^cACCESS Linnaeus Centre and Department of Automatic Control, KTH Royal Institute of Technology, Stockholm, Sweden; ^dASRI, Department of Electrical and Computer Engineering, Seoul National University, Seoul, Republic of Korea

ABSTRACT

Heavy-duty vehicle platooning has received much attention as a method to reduce fuel consumption by keeping inter-vehicle distance short. When a platoon follows a fuel-optimal velocity profile calculated using preview road slope information, significant improvement in the fuel economy occurs. To calculate the optimal velocity in the existing method, however, platoon should acquire expensive road slope data in advance. As an alternative, we propose a road slope estimation method, which enables platoon to calculate the optimal velocity profile without the usage of actual road slope data. Other major challenges in platoon operation include overcoming the effect of the vehicle model uncertainties and external disturbances for ensuring the control performance. The most significant part of the disturbances arises from slopes along a route. Existing method for reducing the effect of the slope employs a feed-forward type compensation in the control loop by combining the vehicle position acquired from GPS and the slope database. However, this method exhibits limitations: the mass of the vehicles in the platoon is uncertain which lowers the accuracy of the feed-forward compensation, and the platoon requires the pre-acquired slope database. To overcome these limitations, we propose an alternative method employing disturbance observer. Simulations of various scenarios are conducted to show the efficacy of the proposed method using the actual road slope data of a Swedish highway.

ARTICLE HISTORY

Received 28 March 2019
Revised 19 November 2019
Accepted 4 December 2019

KEYWORDS

Heavy-duty vehicle platoon;
road slope estimation; robust
control; disturbance observer

1. Introduction

The transportation of goods has been fundamental to the world economic growth and, following the projected GDP annual growth of 2.6 %, the demand for road freight transportation is expected to almost triple by 2050. However, such an increase is leading to the rise of fossil fuel consumption and environmental hazards due to the emission of

greenhouse gases. Although the need for energy efficiency becomes larger, CO₂ emissions from surface (road and rail) transportation are expected to rise by 70 % in the next 30 years [1,2]. This is considered unsustainable and multiple novel technologies are under study to contrast the predicted increase. Vehicle platooning is receiving increasing attention as an effective means to reduce fuel consumption and consequently greenhouse gas emissions of heavy-duty vehicles [3]. Platooning is a smart car solution that can reduce the aerodynamic drag experienced by vehicles by letting groups of vehicles drive at a short inter-vehicular distance. In multiple experimental studies [4–6], it was reported that the aerodynamic drag acting on heavy-duty vehicles is not negligible and, when vehicles travel at a short inter-vehicular distance, it can be significantly reduced, resulting in fuel saving of about 10%.

Research on platooning is not new and dates back to the 1960s. The first works were mostly theoretical and focused on the issue of string stability, i.e. the attenuation of disturbances along the string of platooning vehicles [7–9]. In the 1990s, the research on platooning received a boost by the creation of the Partners in Advance Transportation Technology (PATH) project, which had as the primary focus the investigation of platooning as a tool to increase highway capacity [10]. Within this project, multiple theoretical and experimental works have been carried. Although it was not the main focus, the tests conducted in controlled settings on heavy-duty vehicles showed the potential of platooning to reduce the vehicle fuel consumption [11,12]. These results have been confirmed by independent experiments [5,13–15] that attributed to platooning fuel saving ranging from 4% to 15%.

In the experiments discussed in [13], the authors pointed out how fuel savings from heavy-duty vehicle platooning are highly affected by road topography. Uphills and downhill have in fact a significant effect on the feasible and optimal speed trajectory that each vehicle can and should follow. In [16], the authors showed that, by following an optimised speed profile that explicitly takes topography information into account, a single heavy-vehicle can save up to 3.5% of fuel. While [16] considered the concept of optimal velocity profile for a single vehicle, more recent works of [17–19] extended this concept to a platoon of vehicles. In [19], for example, the authors propose a cooperative look ahead control architecture that includes a platoon coordinator as an upper layer and a Model Predictive Controller (MPC)-based vehicle control as a lower layer. The platoon coordinator uses dynamic programming [20] to calculate a velocity profile for least fuel consumption of the platoon taking into account the slope and travel time constraints. The MPC-based lower layer ensures that each vehicle tracks such velocity profile, while guaranteeing safety by deploying a collision avoidance strategy.

In this paper, we discuss a few aspects of [19] that can be improved. First, the dependency of the controller on the slope data which is used in the upper layer to compute the velocity profile and in the lower layer to compute the estimate of the disturbance due to the slope requires accurate topography information. Such information can be very costly and, in some cases, unavailable. Second, the robustness of the tracking control in the lower layer, where currently only the effect of slope is compensated in feed-forward manner using the slope data, can be improved against model uncertainties such as vehicle mass variations and other disturbances. This paper proposes a Disturbance Observer (DOB)-based approach in order to improve the above-mentioned aspects. DOB is known as one of the powerful tools for robust control and has been successfully applied to many

practical problems in various fields [21–25]. Using control input and sensor measurement, DOB calculates disturbance estimates, rejects the disturbances and also compensates model uncertainties of plant. We follow the platoon architecture proposed in [19], but we deploy a DOB-based controller instead of MPC. Furthermore, in the platoon operations, the dominant disturbance acting on the system comes from the road slope. This means that the slope information can be extracted from the disturbance estimates by DOB. Hence, road slope information along the route can be constructed by combining DOB output and GPS data. The slope estimate may not be accurate in absolute values due to uncertainty in the vehicle mass. However, the estimated profile is proportional to the actual slope along the route, which is enough information to be used in the upper layer to compute the optimal velocity profile for fuel savings. In addition, DOB enhances robustness in the lower layer against model uncertainties such as vehicle mass variations and disturbances.

It should be pointed out that various methods have been used in the literature to estimate road slope. Reference [26] uses a Kalman filter to compute a road slope estimation to be used in the look-ahead vehicle controller. The authors of [27] developed a road slope estimation algorithm based on a GPS receiver, automotive onboard sensors and a vehicle model. To allow adaptation to various slope conditions, a probabilistic data association filter and an interacting multiple model filter were used. The work of [28] developed a method capable of estimating longitudinal velocity and road slope in hybrid electric vehicles employing early detection of excessive wheel slip. Reference [29] proposes a method capable of estimating road slope and vehicle mass in hybrid electric bus through a hybrid algorithm combining an extended Kalman filter and a recursive least square. Reference [30] proposes a slope estimation method based on measurements from an IMU and an orientation filter. To evaluate the proposed method, the authors conducted comparison with pre-acquired high-resolution road slope data. These methods differ from the one proposed in this paper in various ways. First, unlike existing methods, this paper uses DOB for slope estimation and its performance was first evaluated. Second, while existing methods [26–30] mainly focused on how road slope can be estimated or measured, we show how the road slope can be used. Indeed, we directly use the estimated slope for optimal velocity profile calculation and generated the optimal velocity through an optimisation-based algorithm. Finally, the estimate is obtained, as a byproduct, from DOB that compensates the disturbance and uncertainty. Therefore, no complicated algorithms tailored for road slope estimation are needed.

The main contributions of this study are twofold: (i) the proposed method computes optimal velocity profile in the upper layer and compensates external disturbances in the lower layer without the purchase of road slope data. (ii) Furthermore, it enhances robustness in the lower layer against mass and other parameter uncertainties.

The outline of the remainder of the paper is organised as follows. In Section 2, we describe the platoon architecture. The vehicle dynamics modelling is presented in Section 3. In Section 4, we introduce the DOB-based vehicle controller and reference generator. In Section 5, we suggest a method for slope data estimation. Also, we show the platoon operation obtained from the integration with the platoon coordinator and compare it with the alternative approach. The conclusion is drawn in Section 6. Finally, the derivation and necessary parameters are included in the Appendix.

2. Platoon architecture

In this section, we briefly discuss the platoon architecture depicted in Figure 1. The architecture is the modified and extended version of the one presented in [19] and consists of Mission Planner (MP), Road DataBase (RDB), Platoon Coordinator (PC), Reference Generators (RG), Vehicle Controllers (VC) and Vehicles (V) denoted by V_1 to V_N where N is the number of V in the platoon. The constants $\bar{v} > 0$, $v_{\min} \geq 0$, $v_{\max} > 0$ are the desired average velocity, the lower and upper velocity limits for the given section of the roadway, respectively. The signal x_i represents the state vector for V_i that contains its position and velocity, i.e. $x_i = [s_i, v_i]^T \in \mathbb{R}^2$ where s_i is the position of the front side of V_i and v_i is the vehicle velocity. The state vector $\hat{x}_i = [\hat{s}_i, \hat{v}_i]^T \in \mathbb{R}^2$ includes \hat{s}_i and \hat{v}_i , which represent the actual measurement values of s_i and v_i with sensor noises. The signals u_i and b_i are the force generated by the powertrain and braking system of V_i and the distance to the preceding vehicle, respectively. In detail, the signal b_i is computed as

$$b_i = \begin{cases} \infty, & i = 1, \\ s_{i-1} - s_i - l_{i-1}, & i = 2, 3, \dots, N, \end{cases} \quad (1)$$

where l_i denotes the length of V_i . The signals $v_{r,i}$ and $s_{r,i}$ are the desired velocity reference and the position reference for V_i , respectively. In this paper, it is assumed that the platoon follows a constant time gap policy [19], which consists in the requirement that the time interval that passes between two consecutive vehicles going through the same point is fixed, i.e.

$$s_i(t) = s_{i-1}(t - \tau_g), \quad (2)$$

where τ_g is the time gap. As argued in [19], the time gap policy is more efficient in terms of the fuel consumption than the space gap policy which requires the vehicles in the platoon to keep a constant distance. Because this paper follows the time gap policy, we represent some signals as a function of position s_i . The signal $v^*(\hat{s})$ stands for the optimal velocity over space for the entire platoon, which is computed by PC taking into account fuel consumption and travel time. The signal $\hat{\alpha}_1(\hat{s})$ is the road slope data computed by V_1 , and $\hat{\alpha}_\Sigma(\cdot)$ represents the stored road slope data profile of $\hat{\alpha}_1(\hat{s})$.

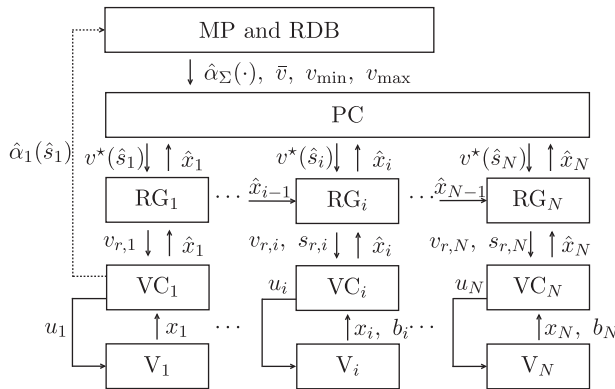


Figure 1. Heavy-duty vehicle platooning architecture.

Mission planner identifies opportunities for platooning by analysing information (e.g. routes, mass, etc.) of vehicles on the road. It is typically implemented off-board in a control centre aimed at coordinating vehicles in the highway road network. In detail, it plans which vehicles will platoon on which section of routes by analysing the trip schedules of vehicles. Once the platooning is decided, MP sends the desired average velocity for the platooning trip, the road slope data for routes and the velocity limits to respect traffic regulation to PC. The desired average velocity \bar{v} is determined by the road property, the weather and traffic conditions, and the travel time requirements. The slope profile of the route $\hat{\alpha}_\Sigma(\cdot)$ may come from a purchased RDB or may be obtained by the platooning vehicles that previously travelled the routes. If RDB does not have slope information for the specific road segment, the platoon will track a constant speed, i.e. the average speed \bar{v} . Although fuel savings are not maximised, DOBs in the platooning vehicles will actively compensate for external disturbances and model uncertainty. Furthermore, the estimated road slope is sent back to RDB such that it can be used by the following platoons.

Platoon coordinator can be implemented either in the off-board control centre or in one of the platooning vehicles. It calculates the optimal velocity for the platoon $v^*(\hat{s})$ using the information given by MP and the states of all N vehicles in the platoon. PC sends the optimal velocity profile and vehicle states to RGs in real time. RG_i modifies the optimal velocity $v^*(\hat{s})$ to the desired velocity reference $v_{r,i}$ and desired position reference $s_{r,i}$ of V_i taking into account the state of the preceding vehicle. VC_i is a feedback controller for V_i . The vehicle controller calculates engine traction force u_i so that v_i and s_i track $v_{r,i}$ and $s_{r,i}$, respectively. Although it is not discussed in this paper, VC_i is also responsible for guaranteeing the safety of the platoon operations by enforcing a constraint on the distance, speed and relative speed of each pair of consecutive vehicle. See [19,32] for details. Finally, there are engine and brake management units included in V_i blocks that receive u_i and regulate the actuators accordingly. Since uncertainties and disturbances exist from the management units, the road condition, and the vehicle mass, VC_i for $i = 2, \dots, N$ must provide robustness.

Controllers rely on the estimation of multiple variables, i.e. vehicle speed, position and inter-vehicular distance. Such variables can be estimated by fusing data from multiple sensors. Vehicle position and speed are typically estimated by fusing data from GPS and measures of the wheels speed. Inter-vehicular distance is typically measured by radar units placed in front of the truck. Such setup has been successfully tested in the experiments reported in [13].

3. Modelling for vehicle dynamics

In this section, we introduce the vehicle dynamics and platoon modelling needed in the design of PC and VC. By Newton's second law, the longitudinal dynamics of single vehicle model is represented as

$$\begin{aligned}\dot{s}_i &= v_i, \\ \dot{v}_i &= \frac{F_{e,i} + F_{b,i} + d_i}{m_i},\end{aligned}\quad (3)$$

where m_i , $F_{e,i}$, $F_{b,i}$, d_i are the mass, the forces generated by the power train and the braking actuator, and the external disturbance of V_i , respectively. The traction force and braking

force are bounded as

$$\begin{aligned} P_{\min,i} &\leq F_{e,i}v_i \leq P_{\max,i}, \\ -m_i\eta_i g\mu_i &\leq F_{b,i} \leq 0, \end{aligned} \quad (4)$$

where the parameters $P_{\min,i}$, $P_{\max,i}$, μ_i , η_i , g are the minimum engine power, the maximum engine power, the road friction coefficient, the braking system efficiency and the gravity acceleration, respectively. The external disturbance d_i consists of three components:

$$d_i = F_{g,i}(\alpha(s_i)) + F_{r,i}(\alpha(s_i)) + F_{d,i}(v_i, b_i), \quad (5)$$

where $F_{g,i}(\alpha(s_i))$ is the gravity force occurring due to the actual road slope $\alpha(s_i)$, $F_{r,i}(\alpha(s_i))$ is the rolling resistance and $F_{d,i}(v_i, b_i)$ is the aerodynamic drag. They are given by

$$\begin{aligned} F_{g,i}(\alpha(s_i)) &= -m_i g \sin(\alpha(s_i)), \\ F_{r,i}(\alpha(s_i)) &= -c_{r,i} m_i g \cos(\alpha(s_i)), \\ F_{d,i}(v_i, b_i) &= -\frac{1}{2} \rho A_v C_D(b_i) v_i^2, \end{aligned} \quad (6)$$

where the parameters $c_{r,i}$, ρ , A_v , $C_D(b_i)$ are the rolling coefficient, the air density, the cross-sectional area and the air drag coefficient of V_i , respectively. It needs to be noted that rigorously speaking, d_i may not be purely external disturbances because $F_{g,i}(\alpha(s_i))$, $F_{r,i}(\alpha(s_i))$ and $F_{d,i}(v_i, b_i)$ are the functions of internal state, i.e. s_i , v_i and b_i . However, we may treat them as the external disturbances in that $F_{g,i}(\alpha(s_i))$, $F_{r,i}(\alpha(s_i))$ and $F_{d,i}(v_i, b_i)$ may not be exactly calculated. Indeed, d_i of (5) is affected by the parameter uncertainties, the mass variation of vehicle, the incorrect slope data, the unreliable scope data and so on. The air drag coefficient is obtained by regressing the experimental data presented in [31] and given by as a function of b_i ,

$$C_D(b_i) = C_{D0} \left(1 - \frac{C_{D1}}{C_{D2} + b_i} \right), \quad (7)$$

where C_{D0} , C_{D1} , C_{D2} are the parameters associated with the aerodynamic drag on follower vehicle. The platoon effect on the lead vehicle is neglected since it is typically significantly smaller than that of the follower vehicles. Here, (7) shows that the short distance between vehicles reduces the aerodynamic resistance. This is a clear reason why platooning of vehicles achieves an improved fuel efficiency.

4. Vehicle controller and reference generator

4.1. Vehicle controller with disturbance observer

We design a vehicle controller VC_i by the combination of outer loop controllers and DOB, and the vehicles are digitally controlled with a Zero-Order Holder (ZOH) and samplers. The block diagram of the designed control system is shown in Figure 2. The transfer function $P_i(s)$ represents the vehicle dynamics from the engine torque to the velocity obtained from the model given in Section 3 and $I_i(s)$ represents an integrator. The discrete time transfer functions $P_{n,i}(z)$, $Q_i(z)$, $C_{v,i}(z)$ and $C_{g,i}(z)$ are the nominal vehicle model of $P_i(s)$,

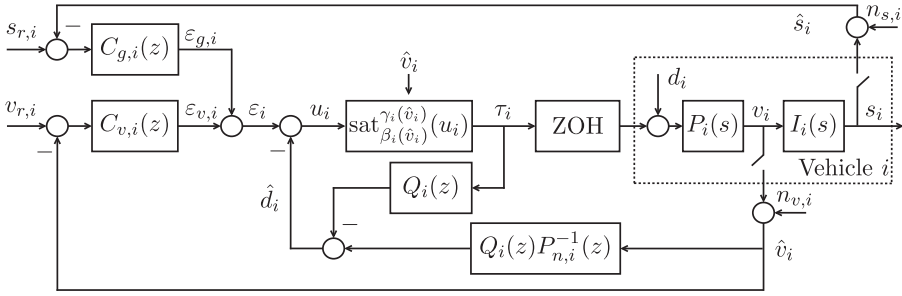


Figure 2. Block diagram of DOB-based vehicle control system.

the low pass filter, the velocity controller and the gap controller of V_i , respectively. The controllers $C_{v,i}(z)$ and $C_{g,i}(z)$ are designed such that the output signals follow the desired references and the gains are chosen using standard techniques such as pole placement or LQR. This paper uses simple gains for $C_{v,i}(z)$ and $C_{g,i}(z)$, respectively, i.e.

$$C_{g,i}(z) = K_{g,i}, \quad C_{v,i}(z) = K_{v,i}, \quad (8)$$

where the gains $K_{g,i}$ and $K_{v,i}$ are designed such that the matrix

$$S_i = \begin{bmatrix} 0 & 1 \\ -\frac{K_{g,i}}{\bar{m}_i} & -\frac{K_{v,i}}{\bar{m}_i} \end{bmatrix} \quad (9)$$

is Hurwitz. Here, \bar{m}_i stands for the nominal mass of V_i . The eigenvalues are placed at -0.1340 and -1.8660 for all vehicles except V_1 . For the leading vehicle V_1 , the gap controller in Figure 2 is not required. The closed loop pole is placed at -2 . The signals τ_i , \hat{d}_i , $n_{v,i}$, $n_{s,i}$ are the actuator engine torque, the estimate of the disturbance and the measurement noises, respectively. The signals \hat{s}_i and \hat{v}_i are the values measured by the GPS and velocity sensors. By following (1), signal \hat{b}_i is defined as $\hat{b}_i = \hat{s}_{i-1} - \hat{s}_i - l_{i-1}$ for $i = 2, \dots, N$. Rest of the signals are the same as those defined in Sections 2 and 3. Specifically, the transfer functions of $P_i(s)$, $I_i(s)$, $P_{n,i}(z)$ and $Q_i(z)$ are given by

$$P_i(s) = \frac{1}{m_i s}, \quad I_i(s) = \frac{1}{s}, \quad P_{n,i}(z) = \frac{T_s}{\bar{m}_i(z-1)}, \quad Q_i(z) = \frac{h_i}{z-1+h_i}, \quad (10)$$

where the parameters T_s and h_i are the sampling time and a tuning parameter, respectively. Here, h_i is positive and less than 1. As h_i becomes closer to 1, DOB estimates exhibit faster transients [25]. The nominal mass \bar{m}_i can be chosen as

$$\bar{m}_i = \frac{1}{2}(m_{\max} + m_{\min}), \quad (11)$$

where m_{\max} and m_{\min} are the permissible maximum and minimum values of the vehicle mass.

The DOB consists of $Q_i(z)P_{n,i}^{-1}(z)$ and $Q_i(z)$ that receive τ_i and \hat{v}_i to compute \hat{d}_i . The disturbance estimate \hat{d}_i from DOB closely follows \hat{d}_i^* , which is given by

$$\hat{d}_i^* = \left(1 - \frac{m_i}{\bar{m}_i}\right) \varepsilon_i + d_i, \quad (12)$$

where ε_i is the sum of the signals from $C_{v,i}(z)$ and $C_{g,i}(z)$. Here, \hat{d}_i^* can be viewed as lumped disturbance including the effect of mass uncertainty and d_i given in (6). Clearly, both external disturbance and the effect of mass uncertainty are compensated by DOB. For more information about DOB, refer to [21–25] and the references therein. The saturation block represents the limits of engine torque and brake force of (4). It is denoted by $\text{sat}_{\beta_i(\hat{v}_i)}^{\gamma_i(\hat{v}_i)}(u_i)$ with $\beta_i(\hat{v}_i)$ and $\gamma_i(\hat{v}_i)$ being the lower and upper limits:

$$\text{sat}_{\beta_i(\hat{v}_i)}^{\gamma_i(\hat{v}_i)}(u_i) = \begin{cases} \beta_i(\hat{v}_i), & u_i < \beta_i(\hat{v}_i), \\ u_i, & \beta_i(\hat{v}_i) \leq u_i \leq \gamma_i(\hat{v}_i), \\ \gamma_i(\hat{v}_i), & u_i > \gamma_i(\hat{v}_i), \end{cases} \quad (13)$$

where the parameters $\beta_i(\hat{v}_i)$ and $\gamma_i(\hat{v}_i)$ are defined as

$$\beta_i(\hat{v}_i) = \frac{P_{\min,i}}{|\hat{v}_i|} - \bar{m}_i \bar{\eta}_i g \bar{\mu}_i, \quad \gamma_i(\hat{v}_i) = \frac{P_{\max,i}}{|\hat{v}_i|}. \quad (14)$$

Here, the parameters $\bar{\eta}_i$ and $\bar{\mu}_i$ are the nominal values of braking system efficiency and road friction coefficient, respectively. The absolute value of \hat{v}_i is used in (14) to ensure that the lower limit $\beta_i(\hat{v}_i)$ is less than the upper limit $\gamma_i(\hat{v}_i)$.

Here, we provide some intuition for the reason why DOB in VC_i can compensate the mass uncertainty and the external disturbances. In the linear region of the saturating actuator, the vehicle velocity v_i is represented by

$$v_i = \frac{1}{m_i s} (\varepsilon_i - \hat{d}_i + d_i). \quad (15)$$

DOB output, i.e. \hat{d}_i closely follows \hat{d}_i^* , and the vehicle velocity of (15) also follows v_i^* , i.e.

$$\begin{aligned} v_i^* &= \frac{1}{m_i s} (\varepsilon_i - \hat{d}_i^* + d_i) \\ &= \frac{1}{m_i s} \left(\varepsilon_i - \left(1 - \frac{m_i}{\bar{m}_i}\right) \varepsilon_i - d_i + d_i \right) \\ &= \frac{1}{\bar{m}_i s} \varepsilon_i. \end{aligned} \quad (16)$$

This shows that DOB estimating \hat{d}_i^* actively compensates the mass uncertainty and the external disturbances and the vehicle V_i is operated with a nominal plant without the uncertainty and disturbances (i.e. $\dot{v}_i \approx \varepsilon_i / \bar{m}_i$). The robustness of the vehicle dynamics is clearly guaranteed through DOB and the external signals, including references, do not affect its robustness.

4.2. Reference generator

We introduce a reference generator to maintain time gap policy. RG calculates the new velocity profile and the new position profile for each vehicle in real time. Without any velocity modification, V_1 in the platoon follows the optimal velocity profile $v^*(\hat{s}_1)$ computed by the high layer. Other vehicles in the platoon follow the modified velocity and position profiles taking the optimal velocity and the current state information of the preceding vehicle into account. The velocity references for V_i are expressed as

$$v_{r,i}(t) = \begin{cases} v^*(\hat{s}_i(t)), & i = 1, \\ \kappa_i v^*(\hat{s}_i(t)) + (1 - \kappa_i) \hat{v}_{i-1}(t - \tau_g), & i = 2, \dots, N, \end{cases} \quad (17)$$

where the parameter $\kappa_i \in (0, 1)$ for $i = 2, \dots, N$ represents the weighting constant. The position reference for the time gap policy is represented by

$$s_{r,i}(t) = \hat{s}_{i-1}(t - \tau_g), \quad i = 2, \dots, N. \quad (18)$$

It should be noted that if the platooning vehicles were able to perfectly track the references, i.e.

$$\hat{v}_i(t) = v_{r,i}(t), \quad \hat{s}_i(t) = s_{r,i}(t), \quad i = 1, \dots, N, \quad (19)$$

the speed and position references $v_{r,i}(t)$ and $s_{r,i}(t)$ would be coherent in spite of the choice of κ_i . In fact, combining Equations (17) and (19), the speed of V_i can be expressed as

$$\hat{v}_i(t) = \left\{ \prod_{p=2}^i (1 - \kappa_p) \right\} v^*(s_1(t - (i-1)\tau_g)) + \sum_{j=2}^i \left\{ \prod_{p=j+1}^i (1 - \kappa_p) \right\} \kappa_j v^*(s_j(t - (i-j)\tau_g)). \quad (20)$$

The derived expression, combined with (18), results in

$$\hat{v}_i(t) = v^*(s_i(t)), \quad (21)$$

i.e. each vehicle is tracking the fuel-optimal reference speed in spite of the choice of κ_i s. Values of κ_i s are however relevant because, due to transitory phases, model uncertainties and disturbances, Equation (19) typically does not hold. Therefore, a value of κ_i close to 0 gives priority to the tracking of the spacing policy. A value of κ_i close to 1 gives a priority to the fuel-efficient speed reference tracking. Note that, in the latter case, the platoon safety is still guaranteed by the safety constraint enforced by VCs. In the simulation introduced in the following section, κ_i s are set to 0.9, aiming therefore to a better tracking of the fuel-optimal speed reference during transitory phases.

5. Main results

In this section, we first present how DOB can be used to extract road slope information from input and output measurements. Second, we test the proposed control architecture in a realistic scenario analysing the effect of uncertainties in the vehicle parameters on the platoon performance. Finally, we compare the performance of the proposed controller with the one of existing solutions.

5.1. Generation of v^* using estimated road slope

We show how to generate v^* using an estimated road slope obtained from DOB output. This pertains to the scenario where RDB does not have any slope data on a roadway segment. A platoon travels the segment initially at constant speed in order to generate v^* for later use. In the illustration, the platoon consists of three vehicles. They are controlled to travel at a constant speed of 22 m/s. The platoon controllers use

$$\bar{m}_1 = \bar{m}_2 = \bar{m}_3 = 40 \text{ t}, \quad (22)$$

while the actual mass are given by

$$m_1 = 40 \text{ t}, \quad m_2 = 36 \text{ t}, \quad m_3 = 44 \text{ t}. \quad (23)$$

Based on the work of [19,26,31,33], other parameters for simulation are selected and shown in Appendix. Uncertainties are assumed for road friction coefficients, braking system efficiencies and rolling coefficients.

The travelling route is the highway stretch between Mariefred and Eskilstuna in Sweden whose actual road topography data are used in the simulation of [19]. The altitude and slope profile along the route are shown in Figure 3(a,b), respectively.

The estimated road slope, denoted by $\hat{\alpha}_1(\hat{s}_1)$, can be obtained from \hat{d}_1 as follows:

$$\hat{\alpha}_1(\hat{s}_1) = \arcsin \left(\frac{\hat{d}_1 + (1/2)\rho A_v C_{D0}(\hat{v}_1)^2}{-\bar{m}_1 g \sqrt{1 + (\bar{c}_{r,1})^2}} \right) - \arctan(\bar{c}_{r,1}), \quad (24)$$

where parameter $\bar{c}_{r,1}$ is the nominal rolling coefficient of V_1 . The slope at the current position, i.e. $\hat{\alpha}_1(\hat{s}_1)$, is constructed by combining \hat{d}_1 (the DOB output) and \hat{s}_1 (the GPS data of V_1). The real time slope data $\hat{\alpha}_1(\hat{s}_1)$ is then integrated into RDB for later use in the form

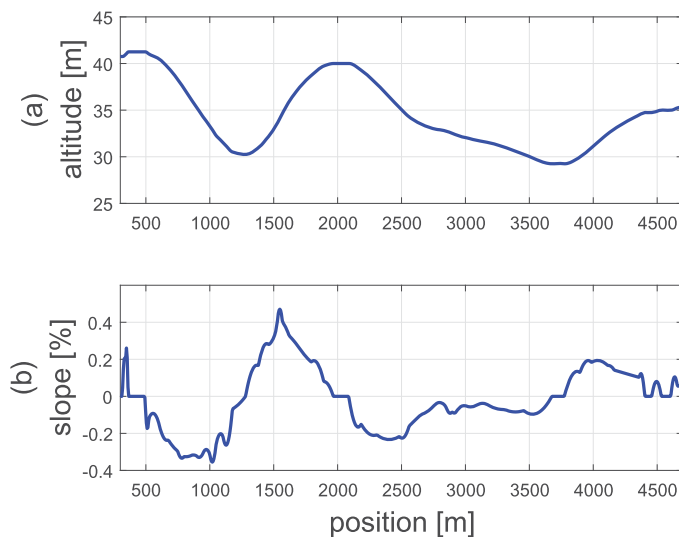


Figure 3. Topography of the highways stretch between Mariefred and Eskilstuna, Sweden.

of slope profile, i.e. $\hat{\alpha}_\Sigma(\cdot)$, which represents the entire slope of a roadway segment. The detailed derivation of (24) is given in Appendix 1.

Figure 4 shows $\hat{\alpha}_1(\hat{s}_1)$ calculated by (24) and its comparison to $\alpha(s_1)$ in Figure 3(b). This clearly shows that $\hat{\alpha}_1(\hat{s}_1)$ and $\alpha(s_1)$ in all area are very similar.

In order to investigate the sensitivity of $\hat{\alpha}_1$ with respect to model uncertainty of V_1 , two more estimates $\hat{\alpha}_{1,A}$ and $\hat{\alpha}_{1,B}$ are obtained from the following cases. The former is obtained from the cases where the actual mass of V_1 is $m_1 = 45$ t, $\bar{m}_1 = 40$ t and the latter is obtained with $m_1 = 35$ t, $\bar{m}_1 = 40$ t. All other parameters in the simulation remain the same for the case of obtaining $\hat{\alpha}_1$.

Figure 5 shows α , $\hat{\alpha}_1$, $\hat{\alpha}_{1,A}$ and $\hat{\alpha}_{1,B}$ all together in the same plot. All three estimated slopes are very similar to the actual slope, even though V_1 has the mass uncertainty of about $\pm 12\%$. These results suggest the robustness of the proposed estimation approach against uncertainties in vehicle mass.

The reason that $\hat{\alpha}_1(\hat{s}_1)$ closely approximates the true slope $\alpha(s_1)$ is as follows. The two are the same if \hat{d}_1 is close to $F_{g,1}$. As discussed in Section 4.1, \hat{d}_1 closely follows \hat{d}_1^* in (12). Note that good tracking performance implies small ε_i , which leaves d_i dominant in \hat{d}_i^* . Again, since $F_{g,1}$ is dominant in d_1 , \hat{d}_1 is close to $F_{g,1}$. Figure 6 shows $F_{g,1}$, d_1 , \hat{d}_1 and \hat{d}_1^* obtained in the simulation. Indeed, the four are almost identical.

Finally, we calculate $v^*(\cdot)$ with PC algorithm proposed in [19] using α , $\hat{\alpha}_1$, $\hat{\alpha}_{1,A}$ and $\hat{\alpha}_{1,B}$. The resulting velocity profiles are shown in Figure 7. The black line shows the optimal velocity computed from the accurate slope data, i.e. α . The green line, blue line and red line show v^* computed using $\hat{\alpha}_1$, $\hat{\alpha}_{1,A}$ and $\hat{\alpha}_{1,B}$, respectively. Even if the variation of about 12% on the vehicle mass occurs, no significant change in v^* is noticed. Some differences do exist in the amplitude. However, such difference does not cause significant variation in the platoon fuel consumption, as it will be shown in Section 5.2. The slopes estimated from (24) give information enough to improve the fuel efficiency.

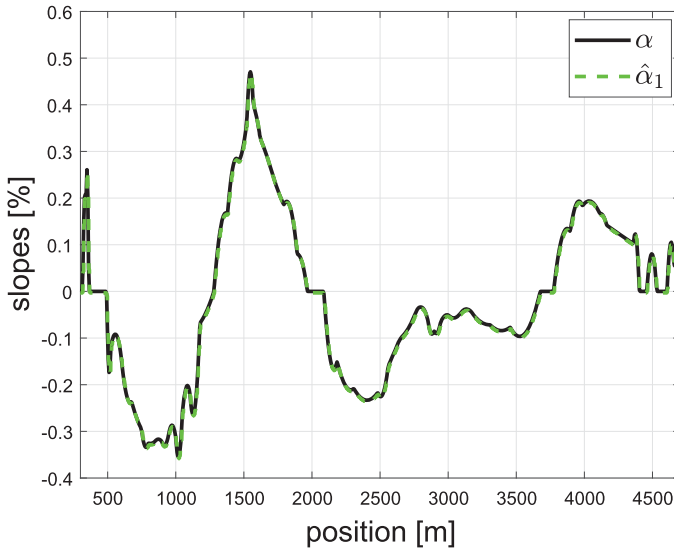


Figure 4. Actual slope and its estimates by V_1 with $\bar{m}_1 = 40$ t and $m_1 = 40$ t.

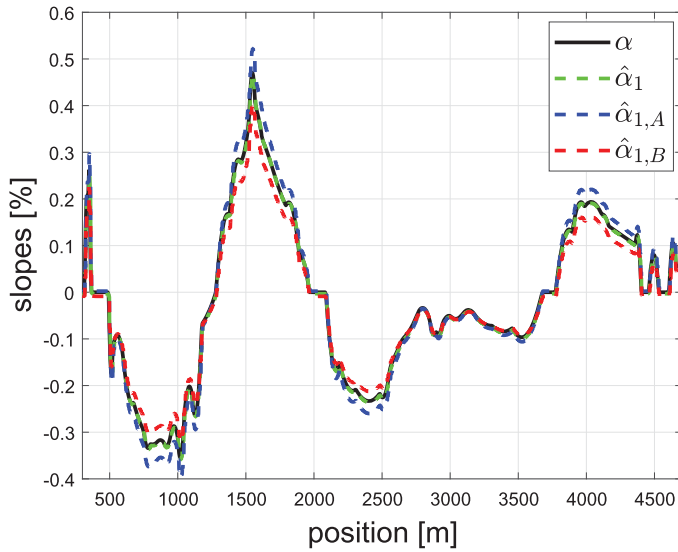


Figure 5. Actual slope and its estimates by several vehicles.

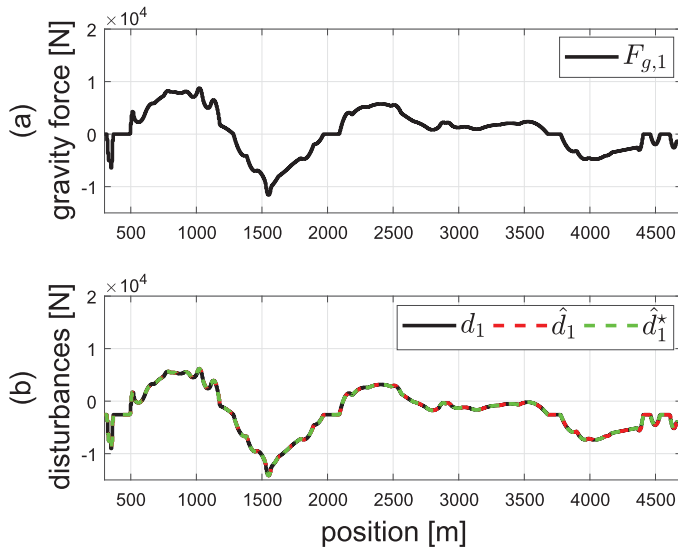


Figure 6. Gravity force, actual disturbance exerted on V_1 and estimated disturbance.

A brief explanation of how PC generates v^* is as follows. Platoon coordinator takes average speed requirement from MP and current vehicle state from all vehicles. By using the available information on the planned route, it generates a unique optimal speed profile which minimises the fuel consumption of the whole platoon, while maintaining a certain average speed. If the slope is not available, PC is not activated. Here, platoon coordinator layer uses a dynamic programming framework to compute optimal velocity profile.

In addition, Figure 8 shows the results for the estimated disturbances of V_2 and V_3 . The DOB outputs \hat{d}_2 and \hat{d}_3 are close to \hat{d}_2^* and \hat{d}_3^* , even if the actual vehicle masses are different with the nominal mass as in (22) and (23).

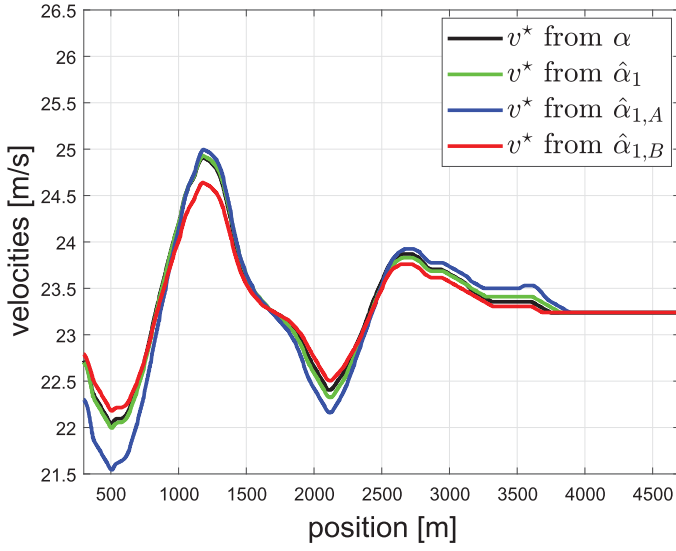


Figure 7. Velocity profiles $v^*(\cdot)$ calculated by PC.

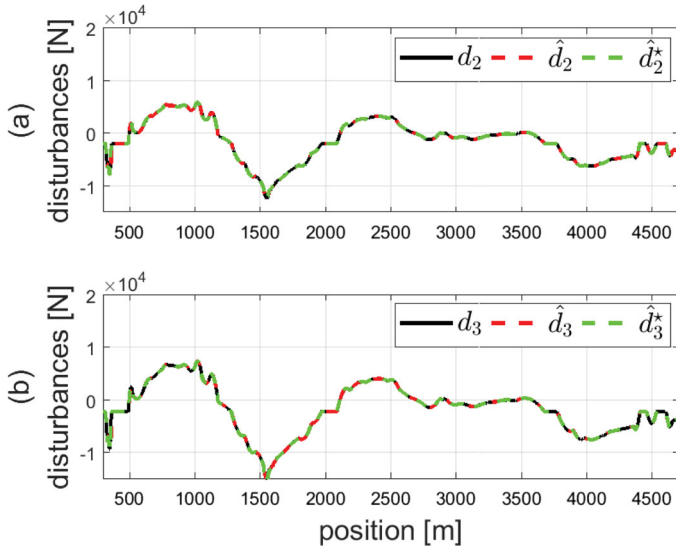


Figure 8. Actual disturbances exerted on V_2 and V_3 and estimated disturbances.

We comment that estimating the road slope is not limited to the first vehicle because all vehicles in the platoon use DOB. As it can be seen from the derivation process of (24) in Appendix A, not only V_1 but also other vehicles have the ability to estimate the road slope. The road slope estimation equation through V_i is given by

$$\hat{\alpha}_i(\hat{s}_i) = \arcsin \left(\frac{\hat{d}_i + (1/2)\rho A_v C_D (\hat{b}_i) (\hat{v}_i)^2}{-\bar{m}_i g \sqrt{1 + (\bar{c}_{r,i})^2}} \right) - \arctan(\bar{c}_{r,i}). \quad (25)$$

However, (25) requires additional measurements (e.g. \hat{b}_i) and it may make estimation process more complex than (24). Limiting the slope estimation to V_1 avoids such complexity. No multiple estimates is necessary since PC uses only one estimate.

5.2. Closed-loop platoon operation

In this section, we show the platoon operation. The parameter setting for the simulation is identical with those in Section 5.1.

We assume that all vehicles in the platoon run on the road displayed in Figure 3(a) and PC generates v^* using the estimated slope $\hat{\alpha}_{1,B}$ (red line of Figure 5). The operation results are shown in Figure 9. First, Figure 9(a) shows that all vehicles in the platoon well track the desired velocity references, although feed-forward type disturbance compensation using actual road slope is not used in the lower layer. Furthermore, Figure 9(b) shows that all vehicles maintain time gap policy without any collision, i.e. $b_2 > 0$, $b_3 > 0$. The corresponding control inputs are shown in Figure 9(c) and all operating points stay in the linear region of (13) without exceeding upper limits of (14). This clearly shows the applicability and efficacy of DOB in the platoon.

Figure 10 shows velocities, distances between vehicles and control inputs for the platoon operation along the same road, but with constant v^* of 22 m/s. This may correspond to an initial travel when slope data is not available, and feed-forward type disturbance compensation [19] is not possible. With the help of DOB, both velocity tracking and time gap are tightly controlled. Responses in Figure 10 show that, although v^* is not optimised for fuel saving by the lack of slope data, the robustness of the platoon is still enhanced.

We compare the total amount of fuel consumption obtained using $\alpha(s_1)$ with those obtained using $\hat{\alpha}_1(\hat{s}_1)$. We use the fuel model introduced in [19,33]. The fuel flow model denoted by δ_i was obtained from a Brake Specific Fuel Consumption (BSFC) mapping that shows an intrinsic relation between the consumed fuel and the generated traction force of the actual truck engine with 400 horsepower. The simplified fuel flow model is expressed as a function of a vehicle speed and a traction force, which is given by

$$\delta_i = \begin{cases} p_{1,i}F_{e,i}v_i + p_{0,i}, & F_{e,i}v_i \geq P_{\min,i}, \\ 0, & F_{e,i}v_i < P_{\min,i}, \end{cases} \quad (26)$$

where parameters $p_{1,i}$ and $p_{0,i}$ are the coefficients associated with the fuel consumption rate.

Figure 11 shows the comparison of five cases. For the convenience of comparison, fuel consumptions in Figure 11 are given in percentage with respect to Case 1. Case 1 shows the fuel consumption when PC does not use road slope data. Case 2 shows fuel consumption when PC uses $\alpha(s_1)$. Cases 3–5 show fuel consumptions where PC is operated using $\hat{\alpha}_1(\hat{s}_1)$ when m_1 is 35 t, 40 t, 45 t, respectively, while \bar{m}_1 is 40 t. They all have similar fuel consumption compared to the case using $\alpha(s_1)$. Therefore, using $\hat{\alpha}_1(\hat{s}_1)$ in PC has as much fuel saving effect as using $\alpha(s_1)$ in PC. We conclude that the actual slope data may not be required anymore in platoon operation.

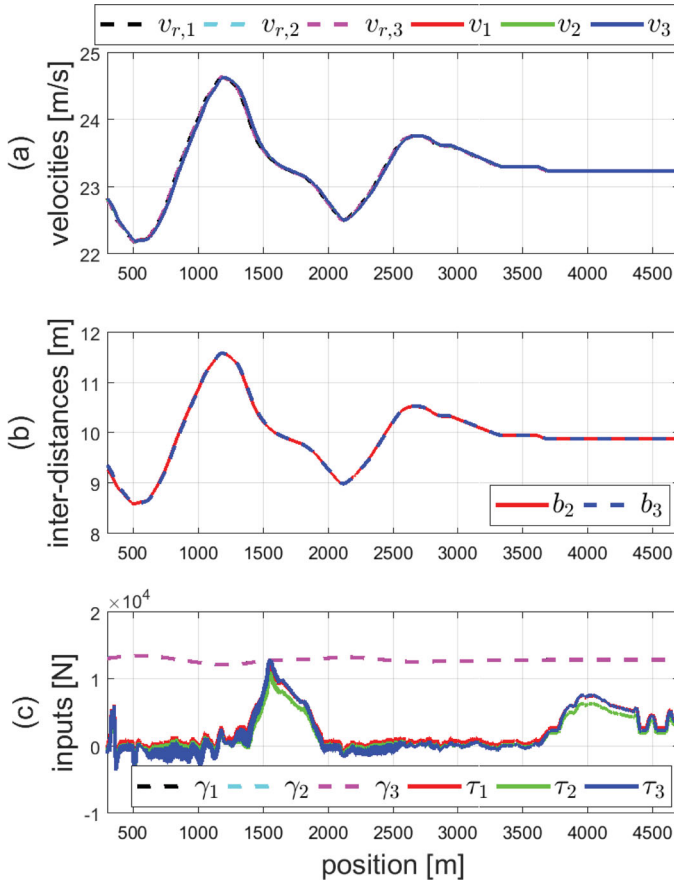


Figure 9. Platoon operation results combined with PC.

5.3. Comparison with alternative solution

In this section, we compare the performance of the proposed controller with the MPC-based approach presented in [19]. The simulation parameters are the same of those in Section 5.2 and the MPC case uses the feed-forward method for the disturbance rejection. The result is shown in Figure 12. Unlike Figure 9, the MPC case is affected by exogenous disturbances and model uncertainties. In particular, as observable in Figure 12(b), the platoon severely deviates from the reference gap policy, even if VC_1 , VC_2 and VC_3 in MPC approach have employed the estimated road slope data.

Here, we compare the proposed approach and the MPC-based platoon of [19] in terms of the fuel consumption and actual simulation time (execution time). The normalised results are displayed in Table 1. What we notice is that the MPC-based platoon of [19] may have lower fuel consumptions than the proposed method. This is because the MPC method introduced in [19] has employed the constraints that use braking only when necessary and we can observe it in Figure 12(c). Although the MPC-based platoon results in a reduced fuel consumption, DOB-based platoon shows multiple advantages: first, VC_1 , VC_2 and VC_3 in the DOB approach do not require the road map data and DOBs in vehicle

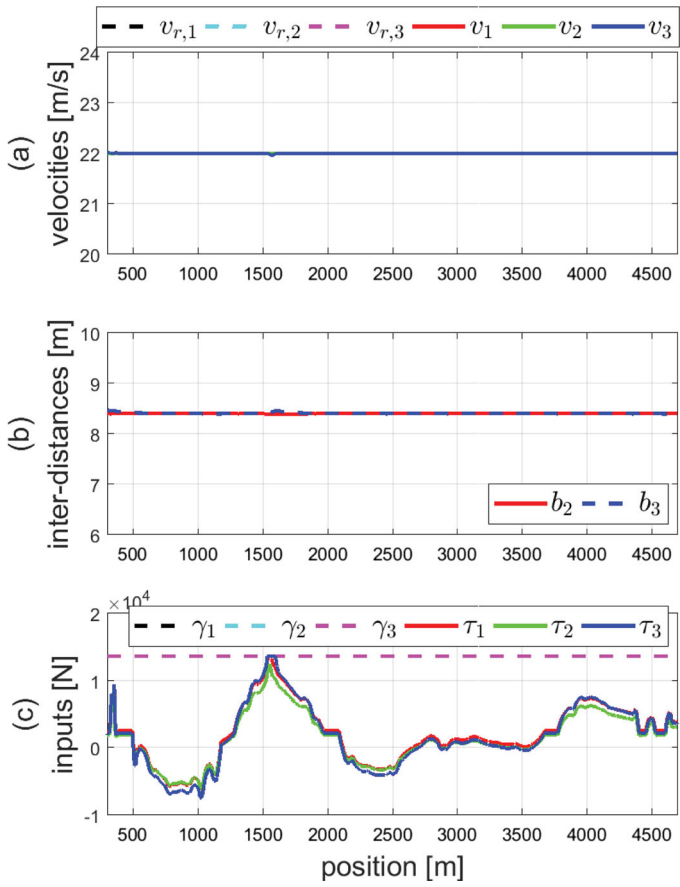


Figure 10. Platoon operation results for constant v^* .

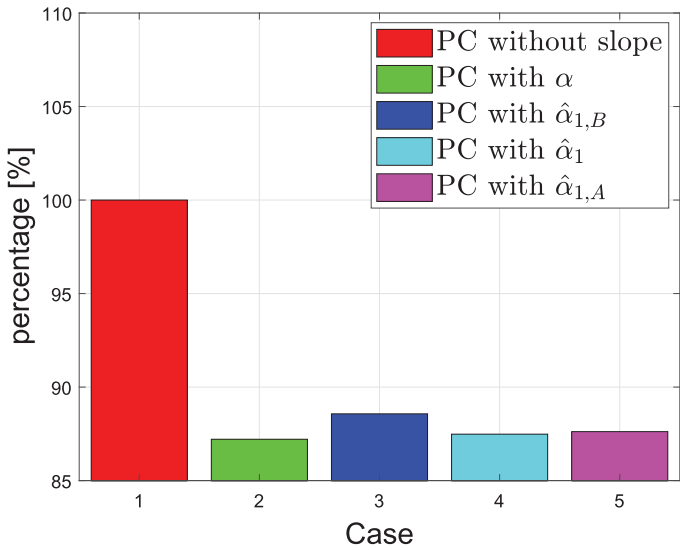


Figure 11. Fuel consumption of the platoon.

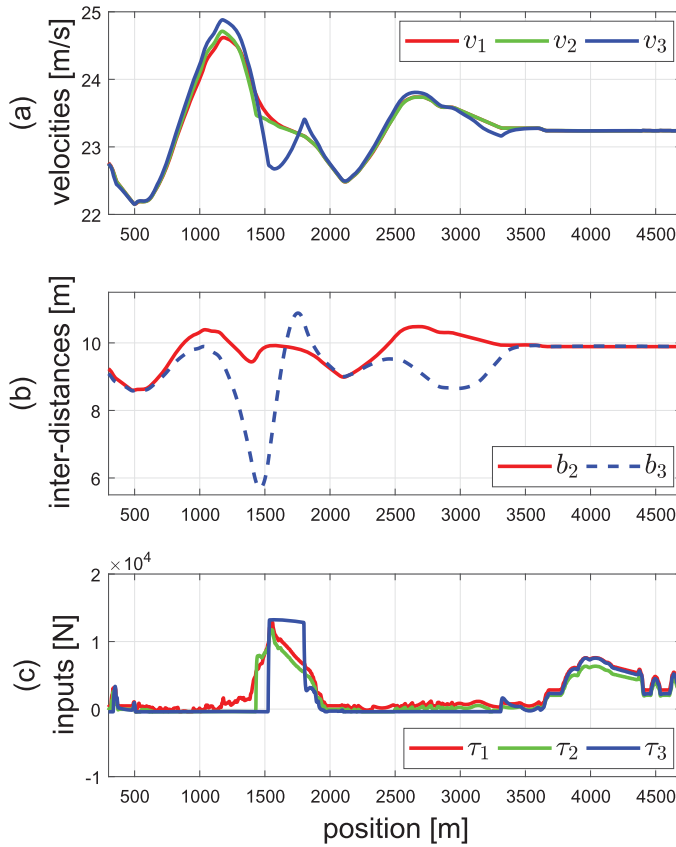


Figure 12. MPC-based platoon operation results.

Table 1. Platoon fuel consumption and actual simulation time for the proposed approach and the MPC approach. The values are normalised with those ones corresponding to the case introduced in Section 5.3 where the PC does not use slope information.

	DOB	MPC
Fuel consumption [%]	88.57	80.82
Simulation time [%]	100	927

can estimate the road data; second, the platoon exhibits better tracking performance under model uncertainties and disturbances; third, DOB-based platoon has lower computation time comparing with MPC.

6. Conclusion

Existing platoon approach requires the actual road slope data and exact model knowledge for calculating velocity profile optimised for fuel saving and for compensating the effect of uphill and downhill in the velocity tracking feedback control. In this paper, a new DOB-based approach is proposed which does not require the actual road slope data and exact

model knowledge. Using DOB-based estimation, the approach achieves both fuel savings and robust velocity tracking performance. The results are illustrated using simulation.

Limitations of current study are summarised as follows. This paper employed a simplified fuel model for calculating fuel consumption. More accurate fuel model needs to be used for more exact calculation. Future work include (DOB based) mass estimation method development, new algorithm development for avoiding unnecessary inefficient braking and achieving therefore better fuel consumption, etc.

Disclosure statement

No potential conflict of interest was reported by the authors.

Funding

This work was partly supported by Institute of Information and Communications Technology Planning and Evaluation (IITP) grant funded by the Korea government (MSIT) (No. 2014-3-00065, Resilient Cyber-Physical Systems Research), partially supported by Global Research Laboratory Program through the National Research Foundation of Korea (NRF-2013K1A1A2A02078326) and also supported in part by R&D Program of the Korea Railroad Research Institute (PK1901B1-1).

ORCID

Yongsoon Eun  <http://orcid.org/0000-0002-2304-7106>

References

- [1] European Commission. EU transport in figures: statistical pocketbook. Technical Report, Brussels. 2018.
- [2] ACEA – European Automobile Manufacturers Association. Reducing CO₂ emissions form heavy-duty vehicles. Technical Report, London. 2017.
- [3] OECD/ITF. ITF transport outlook. Technical Report, Paris. 2017.
- [4] Bonnet C, Fritz H. Fuel consumption reduction in a platoon: experimental results with two electronically coupled trucks at close spacing. SAE Technical Paper Series. 2000.
- [5] Lammert MP, Duran A, Diez J, et al. Effect of platooning on fuel consumption of class 8 vehicles over a range of speeds, following distances, and mass. SAE Int J Commercial Veh. 2014;7(2):626–639.
- [6] Alam A, Mårtensson J, Johansson KH. Experimental evaluation of decentralized cooperative cruise control for heavy-duty vehicle platooning. Control Eng Pract. 2015;38:11–25.
- [7] Peppard LE. String stability of relative-motion PID vehicle control systems. IEEE Trans Automat Contr. 1974;19(5):579–581.
- [8] Dunbar WB, Murray RM. Distributed receding horizon control for multi-vehicle formation stabilization. Automatica. 2006;42(4):549–558.
- [9] Naus GJL, Vugts RPA, Ploeg J, et al. String-stable CACC design and experimental validation: a frequency-domain approach. IEEE Trans Veh Tech. 2010;59(9):4268–4279.
- [10] Shladover SE. PATH at 20-History and major milestones. IEEE Trans Intell Transp Syst. 2007;8(4):584–592.
- [11] Shladover SE, Lu XY, Song B, et al. Demonstration of automated heavy-duty vehicles. California PATH Research Report. 2005.
- [12] Lu XY, Shladover SE, Hedrick JK. Heavy-duty truck control short inter-vehicle distance following. Proceedings of the American Control Conference. 2004, 4722–4727.
- [13] Alam A, Besselink B, Turri V, et al. Heavy-duty vehicle platooning for sustainable freight transportation: a cooperative method to enhance safety and efficiency. IEEE Control Sys. 2015;35(6):34–56.

- [14] Roeth M. CR england peloton technology platooning test Nov 2013. North American Council for Freight Efficiency, Fort Wayne, IN. 2013.
- [15] McAuliffe B, Croken M, Ahmadi-Baloutaki M, et al. Fuel-economy testing of a three-vehicle truck platooning system. Technical Report, Berkeley, CA. 2017.
- [16] Hellström E, Ivarsson M, Åslund J, et al. Look-ahead control for heavy trucks to minimize trip time and fuel consumption. *Control Eng Pract.* 2009;17(2):245–254.
- [17] Murgovski N, Egardt B, Nilsson M. Cooperative energy management of automated vehicles. *Control Eng Pract.* 2016;57:84–98.
- [18] Kaku A, Kamal AS, Mukai M, et al. Model predictive control for ecological vehicle synchronized driving considering varying aerodynamic drag and road shape information. *SICE J Control Measurement Sys Integr.* 2013;6(5):299–308.
- [19] Turri V, Besselink B, Johansson KH. Cooperative look-ahead control for fuel-efficient and safe heavy-duty vehicle platooning. *IEEE Trans Control Syst Technol.* 2017;25(1):12–28.
- [20] Bellman RE. *Dynamic programming.* Princeton, NJ: Princeton University Press; 1957.
- [21] Shim H, Jo NH. An almost necessary and sufficient condition for robust stability of closed-loop systems with disturbance observer. *Automatica.* 2009;45(1):296–299.
- [22] Back J, Shim H. Adding robustness to nominal output feedback controllers for uncertain nonlinear systems: a nonlinear version of disturbance observer. *Automatica.* 2008;44(10):2528–2537.
- [23] Shim H, Joo Y. State space analysis of disturbance observer and a robust stability condition. *Proceedings of IEEE Conference on Decision and Control.* 2007. p. 2193–2198.
- [24] Shim H, Park G, Joo Y, et al. Yet another tutorial of disturbance observer: robust stabilization and recovery of nominal performance. *Control Theory Tech.* 2016;14(3):237–249.
- [25] Park G, Joo Y, Lee C, et al. On robust stability of disturbance observer for sampled-data systems under fast sampling: an almost necessary and sufficient condition. *Proceedings of IEEE Conference on Decision and Control.* 2015. p. 7536–7541.
- [26] Sahlholm P, Johansson KH. Road grade estimation for look-ahead vehicle control using multiple measurement runs. *Control Eng Pract.* 2010;18(11):1328–1341.
- [27] Jo K, Kim J, Sunwoo M. Real-time road-slope estimation based on integration of onboard sensors with GPS using an IMM-PDA filter. *IEEE Trans Int Transp Sys.* 2013;14(4):1718–1732.
- [28] Klomp M, Gao Y, Bruzelius F. Longitudinal velocity and road slope estimation in hybrid electric vehicles employing early detection of excessive wheel slip. *Veh Sys Dyn.* 2014;52:172–188.
- [29] Sun Y, Li L, Yan B, et al. A hybrid algorithm combining EKF and RLS in synchronous estimation of road grade and vehicle' mass for a hybrid electric bus. *Mech Syst Signal Process.* 2016;68-69:416–430.
- [30] Jauch J, Masino J, Staiger T, et al. Road grade estimation with vehicle-based inertial measurement unit and orientation filter. *IEEE Sens J.* 2018;18(2):781–789.
- [31] Hucho WH. *Aerodynamics of road vehicles.* Oxford: Butterworth-Heinemann; 1987.
- [32] Alam A, Gattami A, Johansson KH, et al. Guaranteeing safety for heavy duty vehicle platooning: safe set computations and experimental evaluations. *Control Eng Pract.* 2014;24:33–41.
- [33] Sandberg T. *Heavy truck modeling for fuel consumption simulations and measurements.* Licentiate Thesis. Sweden: Linköping University; 2001.

Appendices

Appendix 1. Derivation of (24)

The external disturbance of V_i , i.e. d_i is represented from (5) and (6) by

$$d_i = -m_i g \sin(\alpha(s_i)) - c_{r,i} m_i g \cos(\alpha(s_i)) - \frac{1}{2} \rho A_v C_D (b_i) (v_i)^2. \quad (A1)$$

The composite formula of trigonometric function and (A1) yield

$$d_i = -m_i g \sqrt{1 + (c_{r,i})^2} \sin(\alpha(s_i) + \arctan(c_{r,i})) - \frac{1}{2} \rho A_v C_D (b_i) (v_i)^2. \quad (A2)$$

Then, slope $\alpha(s_i)$ can be derived from (A2) as

$$\alpha(s_i) = \arcsin \left(\frac{d_i + (1/2)\rho A_v C_D(b_i)(v_i)^2}{-m_i g \sqrt{1 + (c_{r,i})^2}} \right) - \arctan(c_{r,i}). \quad (\text{A3})$$

Substitute unknown variables in (A3), i.e. $\alpha(s_i)$, m_i , d_i , b_i and $c_{r,i}$, into nominal values and measured signals, i.e. $\hat{\alpha}_i(\hat{s}_i)$, \bar{m}_i , \hat{d}_i , \hat{b}_i , and $\bar{c}_{r,i}$. Then, we have

$$\hat{\alpha}_i(\hat{s}_i) = \arcsin \left(\frac{\hat{d}_i + (1/2)\rho A_v C_D(\hat{b}_i)(\hat{v}_i)^2}{-\bar{m}_i g \sqrt{1 + (\bar{c}_{r,i})^2}} \right) - \arctan(\bar{c}_{r,i}). \quad (\text{A4})$$

Recall (7). The first vehicle, i.e. V_1 has $b_1 \approx \hat{b}_1 \approx \infty$ and $C_D(\infty) = C_{D0}$. By combining them with (A4), we complete it.

Appendix 2. Parameter setting for simulation

A.1 Parameters of first vehicle, second vehicle and third vehicle

	First vehicle	Second vehicle	Third vehicle
Actual mass (m_i)	40 t	36 t	44 t
Nominal mass (\bar{m}_i)	40 t	40 t	40 t
Braking system efficiency (η_i)	1	0.98	0.99
Nominal braking system efficiency ($\bar{\eta}_i$)	0.985	0.985	0.985
Road friction coefficient (μ_i)	0.77	0.78	0.81
Nominal road friction coefficient ($\bar{\mu}_i$)	0.8	0.8	0.8
Rolling coefficient ($c_{r,i}$)	0.0028	0.0030	0.0032
Nominal rolling coefficient ($\bar{c}_{r,i}$)	0.0030	0.0030	0.0030
Maximum engine power ($P_{\max,i}$)	300 kW	300 kW	300 kW
Minimum engine power ($P_{\min,i}$)	-9 kW	-9 kW	-9 kW
Vehicle length (l_i)	18 m	18 m	18 m
Tuning parameter for DOB (h_i)	1	1	1
Fuel flow model coefficient ($p_{0,i}$)	5.919×10^{-5}	5.919×10^{-5}	5.919×10^{-5}
Fuel flow model coefficient ($p_{1,i}$)	5.357×10^{-8}	5.357×10^{-8}	5.357×10^{-8}
Weighting value (κ_i)		0.90	0.90
Gap controller ($K_{g,i}$)		1×10^4	1×10^4
Velocity controller ($K_{v,i}$)	8×10^4	8×10^4	8×10^4

A.2 Common parameters

Air density (ρ)	1.225 kg/m ³
Cross-sectional area (A_v)	9.487 m ²
Nominal drag coefficient (C_{D0})	0.53
First drag reduction coefficient (C_{D1})	14.67 m ⁻¹
Second drag reduction coefficient (C_{D2})	26.67 m
Time gap (τ_g)	1.2 s
Sampling time (T_s)	0.05 s
Upper velocity limit (v_{\max})	25 m/s
Permissible minimum vehicle mass (m_{\min})	35 t
Permissible maximum vehicle mass (m_{\max})	45 t
Gravity acceleration (g)	9.8 m/s ²